Coulomb three-body effects in low-energy impact ionization of H(1s)

J. Röder,[1] J. Rasch,[2] K. Jung,[1] Colm T. Whelan,[2] H. Ehrhardt,[1] R. J. Allan,[3] and H. R. J. Walters[4]
[1]*Fachbereich Physik, Universität Kaiserslautern, Erwin Schrödinger Straβe, 67663 Kaiserslautern, Germany*
[2]*Department of Applied Mathematics and Theoretical Physics, University of Cambridge, Silver Street, Cambridge CB3 9EW, England*
[3]*Daresbury Laboratory, Warrington WA4 4AD, England*
[4]*Department of Applied Mathematics and Theoretical Physics, The Queen's University of Belfast, BT7 1NN Belfast, Northern Ireland*
(Received 8 May 1995)

The different kinematical and geometrical arrangements that may be used in (e,2e) studies are briefly reviewed. The ionization of H(1s) is considered, and within the confines of a relatively simple theoretical model, it is shown how to define experimental setups where one may extract information on the role of Coulomb three-body effects in the incident and final channels. Theoretical and experimental results are presented for coplanar constant geometry where the focus is primarily on incident channel effects.

PACS number(s): 03.65.Nk

I. INTRODUCTION

The electron-impact ionization of atomic hydrogen is one of the purest examples of the Coulomb three-body problem in atomic physics. Three-body effects manifest themselves in both the incident and final channels; exchange, distortion, polarization-correlation and post-collisional interactions all play a part, as effects in themselves, and in their interference with one another.

In this paper we present a joint theoretical-experimental study of H(1s), at impact energies of 54.4 eV and less in a variety of geometrical and kinematical arrangements. We will show how the different effects contribute, and consider how by suitable choice of the geometry and kinematics one may make one effect dominant. We consider several different geometrical arrangements where both the outgoing electrons have equal energies. In particular a whole set of additional measurements have been performed in such an energy sharing setup where the angle between the two outgoing electrons is held fixed and the triple differential cross section (TDCS) is given as a function of one of the scattered electrons. This geometry has been proposed by Whelan and coworkers [1,2] as an ideal arrangement for studying incident channel effects at low energies, and distortion effects at relativistic energies [3].

A second energy sharing arrangement is the conventional coplanar symmetric geometry where both electrons are detected with the same angle left and right of the beam direction. The TDCS is given as a function of this angle. We also consider coplanar asymmetric geometry, where the energy of the outgoing electrons are no longer equal; the faster of the two electrons is detected at a fixed angle ϑ_f, while the TDCS is given as a function of the second angle ϑ_s.

II. THEORY

Suppose we have an electron with momentum $\mathbf{k}_0$ and energy E_0, which collides with a hydrogen atom in its ground state; after the collision two electrons, one with momentum $\mathbf{k}_f$ and energy E_f, and a second with momentum $\mathbf{k}_s$ and energy E_s, are detected in coincidence. All three momentum vectors are lying in a plane for the results we present here.

For the T-matrix element of such a process, basic collision theory [4] would then give

$$T(\mathbf{k}_s,\mathbf{k}_f)=\langle e^{i\mathbf{k}_f\cdot\mathbf{r}_f}e^{i\mathbf{k}_s\cdot\mathbf{r}_s}|V_f(\mathbf{r}_s,\mathbf{r}_f)|\Psi_i^+(\mathbf{r}_s,\mathbf{r}_f)\rangle,$$

where the outgoing electrons are represented by plane waves, and $|\Psi_i^+\rangle$ denotes the complete scattering wave function with outgoing scattered wave boundary conditions

$$|\Psi_i^+(\mathbf{r}_s,\mathbf{r}_f)\rangle=[1+(E-H+i\epsilon)^{-1}]|e^{i\mathbf{k}_0\cdot\mathbf{r}_f}\varphi_0(\mathbf{r}_s)\rangle.$$

$\varphi_0(\mathbf{r}_s)$ is the bound-state wave function of the hydrogen atom in the initial state. The final-state interaction in the T-matrix element is of the form

$$V_f(\mathbf{r}_s,\mathbf{r}_f)=(V_s+V_f+V_{sf}),$$

where

$$V_s=-\frac{1}{r_s},\quad V_f=-\frac{1}{r_f},\quad V_{sf}=\frac{1}{r_{sf}},\quad r_{sf}=\|\mathbf{r}_s-\mathbf{r}_f\|.$$

In Refs. [5] and [6] it is shown that, quite generally, the direct scattering amplitude for electron-impact ionization of atomic hydrogen can be recast into the form

$$f(\mathbf{k}_f,\mathbf{k}_s)=\langle\chi_a^-(\mathbf{k}_f,\mathbf{r}_f)\chi_b^-(\mathbf{k}_s,\mathbf{r}_s)|V_f+V_s+V_{sf}-V_a(\mathbf{r}_f)-V_b(\mathbf{r}_s)|\Psi_i^+(\mathbf{r}_f,\mathbf{r}_s\rangle, \tag{1}$$

where $\chi_{a,b}^-(\mathbf{k},\mathbf{r})$ satisfies

$$[-\tfrac{1}{2}\nabla^2+V_{a,b}(\mathbf{r})-\tfrac{1}{2}k^2]|\chi_{a,b}(\mathbf{r})\rangle=0,$$

with ingoing wave boundary conditions for the distorting potentials V_a and V_b. For the purposes of this paper we will take $V_a=V_f$ and $V_b=V_s$, i.e., χ_a^-, χ_b^- become continuum Coulomb waves with ingoing boundary conditions, i.e., $\chi^-(\mathbf{r})$ is given by

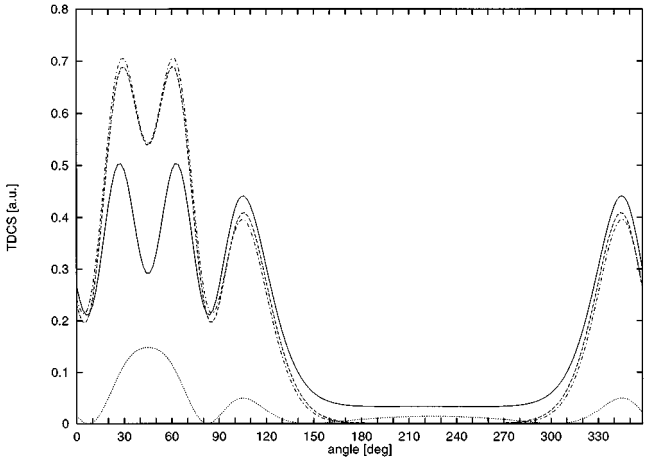

FIG. 1. TDCS in coplanar energy sharing geometry at 25.0 eV; the angle between the two outgoing electrons is fixed at an angle of 90°. Shown are DWBA, DWBA plus polarization, and a series of model calculations: DWBA with polarization, (solid line), standard DWBA (dashed), the plane wave in the incident channel (dashed-dotted), and plane waves in the final channel (dotted).

$$\frac{1}{(2\pi)^{3/2}}\, e^{-(\pi/2k)}\Gamma\left(1+i\,\frac{1}{k}\right)e^{i\mathbf{k}\cdot\mathbf{r}} \times {}_1F_1\left(-i\,\frac{1}{k};1;-ikr-i\mathbf{k}\cdot\mathbf{r}\right).$$

The distorted-wave Born approximation is defined by replacing

$$|\Psi_i^+(\mathbf{r}_s,\mathbf{r}_f)\rangle = |\chi_i^{+,(S)}(\mathbf{r}_f)\varphi_0(\mathbf{r}_s)\rangle.$$

S is the total spin, and

$$\chi_i^{+,(S)}(\mathbf{r}_f)\varphi_0(\mathbf{r}_s)+(-)^S\chi_i^{+,(S)}(\mathbf{r}_s)\varphi_0(\mathbf{r}_f)$$

is the singlet-triplet wave function for elastic scattering by the hydrogen atom in the state φ_0. We use two different potentials to generate the distorted waves: (a) the static-exchange potential, and (b) the static-exchange potential modified by the addition of the polarization potential defined in our earlier papers [2]; i.e.,

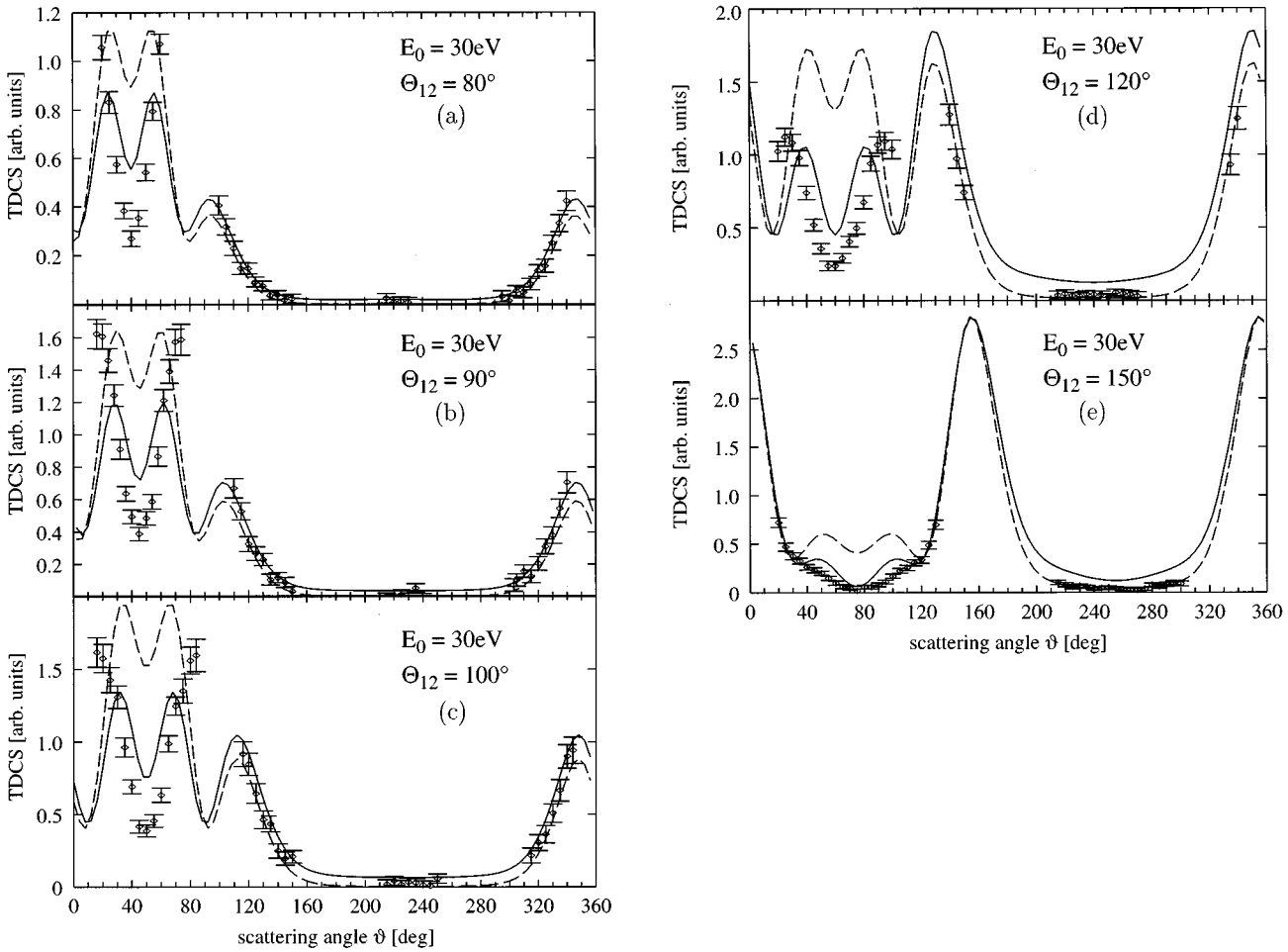

FIG. 2. TDCS in coplanar energy sharing geometry at an impact energy of $E_0=30.0$ eV. Experimental data are internormalized but relative, therefore all experimental data are scaled by the same overall factor to give the best fit to theory. Curves in all figures: DWBA with polarization and PCI effects included (solid line); and standard DWBA with PCI effects included (dashed). Both calculations are scaled by the N_{ee} factor such that the TDCS is given in arbitrary units. The angle between the two outgoing electrons is fixed at angles of (a) 80°, (b) 90°, (c) 100°, (d) 120°, and (e) 150°.

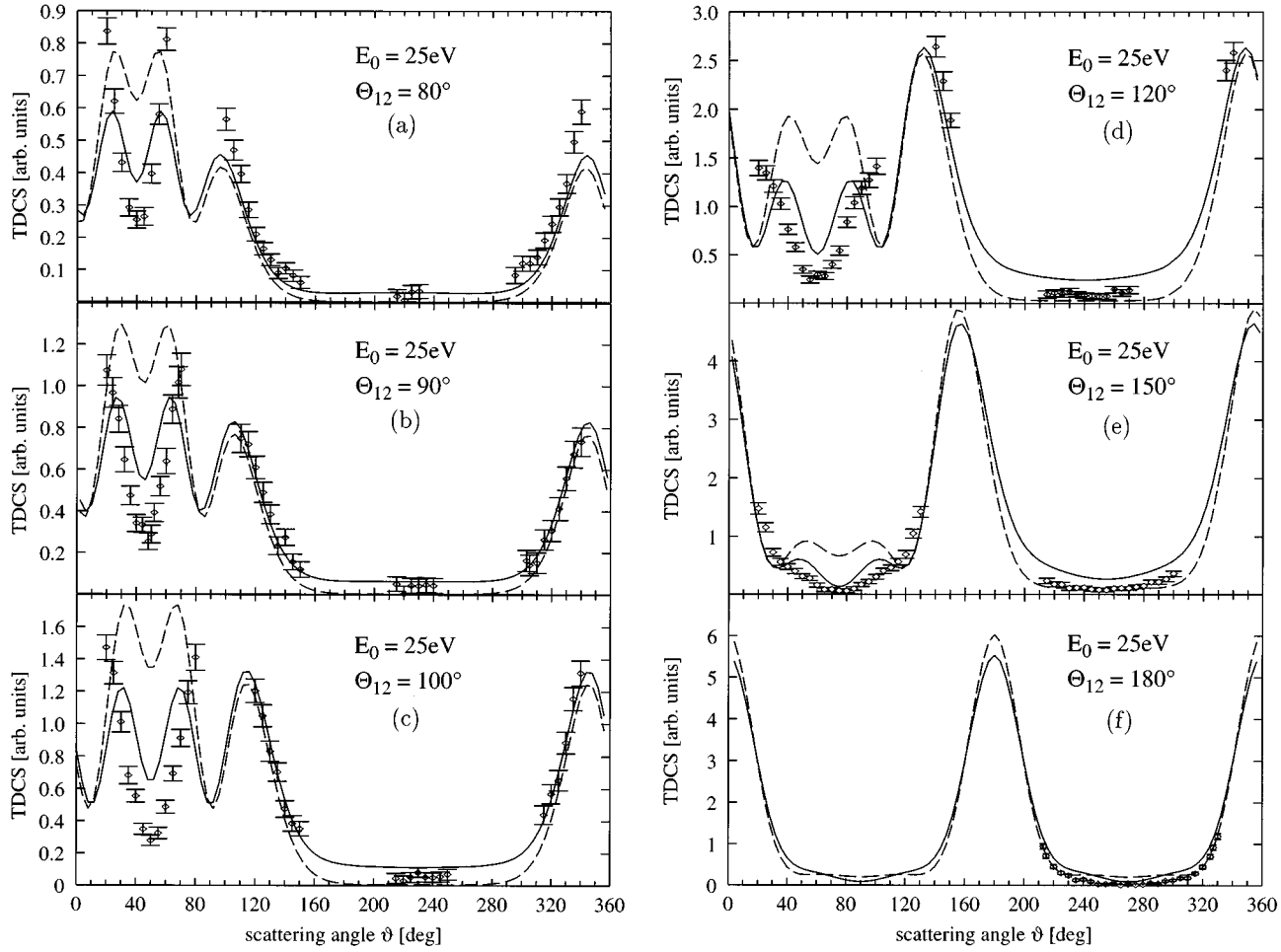

FIG. 3. TDCS in coplanar energy sharing geometry at an impact energy of $E_0=25.0$ eV. Experimental data are internormalized but relative, therefore all experimental data are scaled by the same overall factor to give the best fit to theory. Curves in all figures: DWBA with polarization and PCI effects included (solid line); and standard DWBA with PCI effects included (dashed). Both calculations are scaled by the N_{ee} factor such that the TDCS is given in arbitrary units. The angle between the two outgoing electrons is fixed at angles of (a) 80°, (b) 90°, (c) 100°, (d) 120°, (e) 150°, and (f) 180°.

$$V=\begin{cases} -\dfrac{\alpha}{2r^4} & r>r_0 \\ -\dfrac{\alpha}{2r_0^4} & r<r_0\,, \end{cases} \tag{2}$$

where $\alpha=4.5$ is the polarizability of neutral H($1s$), and r_0 was taken to be 1.2239 (in a.u.). We remark that the value for r_0 we use is not a free parameter, rather it was fixed by Whelan *et al.* [2] by comparison with earlier results on helium.

The direct and exchange amplitudes may now be written as

$$f^S(\mathbf{k}_s,\mathbf{k}_f)=\left\langle \chi_a^-(\mathbf{r}_f)\chi_b^-(\mathbf{r}_s)\left|\frac{1}{r_{sf}}\right|\chi_i^{+,(S)}(\mathbf{r}_f)\varphi_0(\mathbf{r}_s)\right\rangle,$$

$$g^S(\mathbf{k}_s,\mathbf{k}_f)=\left\langle \chi_a^-(\mathbf{r}_s)\chi_b^-(\mathbf{r}_f)\left|\frac{1}{r_{sf}}\right|\chi_i^{+,(S)}(\mathbf{r}_f)\varphi_0(\mathbf{r}_s)\right\rangle.$$

The triple differential cross section is then given by

$$\frac{d^3\sigma^{\mathrm{DWBA}}}{d\Omega_s d\Omega_f dE}=4(2\pi)^4\frac{k_s k_f}{k_0}\left(\tfrac{3}{4}|f^{(1)}-g^{(1)}|^2+\tfrac{1}{4}|f^{(0)}+g^{(0)}|^2\right), \tag{3}$$

where we have summed over all initial, and averaged over all final, spin states. We note that had we used the exact wave function $|\Psi_i^+\rangle$ there would have been no distinction between the singlet functions $f^{(0)},g^{(0)}$ and triplet functions $f^{(1)},g^{(1)}$, but because of the nature of the approximate wave function (2) we obtain different amplitudes for the singlet and triplet cases [7].

In the generation of the incident channel distorted waves we use the Furness-McCarthy local exchange potential [8,9]

$$V_{\mathrm{exchange}}=\frac{1}{2}\left[\frac{1}{2}k^2-V-\sqrt{\left(\tfrac{1}{2}k^2-V\right)+\beta|R_{1s}|^2}\right], \tag{4}$$

where R_{1s} is the radial part of the $1s$ orbital, $\beta=2$ for triplet scattering, $\beta=-2$ for singlet scattering. V can be either the static potential of the hydrogen atom or the static plus polarization potential. If we use the static potential there is a range

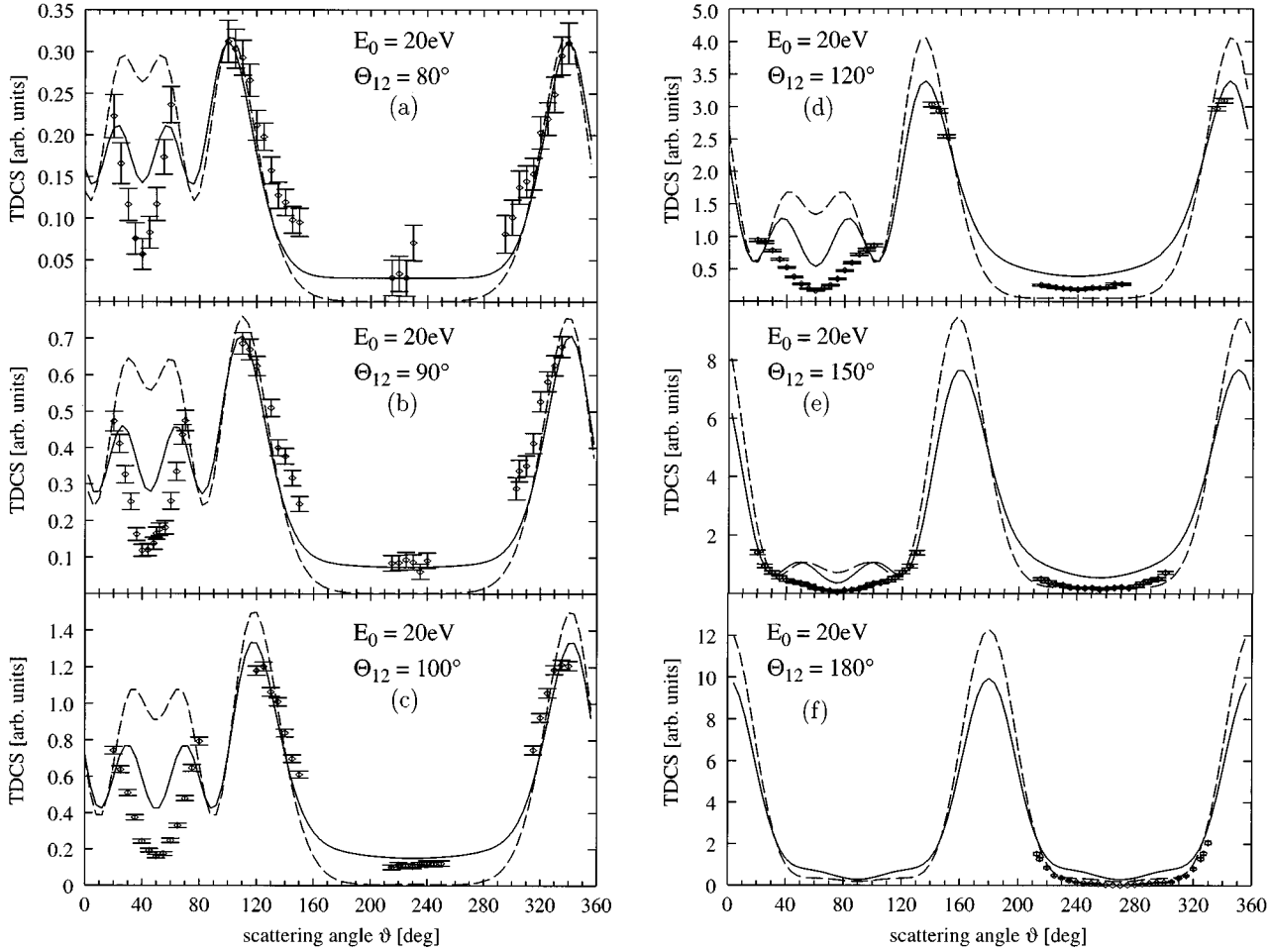

FIG. 4. TDCS in coplanar energy sharing geometry at an impact energy of $E_0 = 20.0$ eV. Experimental data are internormalized but relative, therefore all experimental data are scaled by the same overall factor to give the best fit to theory. Curves in all figures: (a) DWBA with polarization and PCI effects included (solid line); and (b) standard DWBA with PCI effects included (dashed). Both calculations are scaled by the N_{ee} factor such that the TDCS is given in arbitrary units. The angle between the two outgoing electrons is fixed at angles of (a) 80°, (b) 90°, (c) 100°, (d) 120°, (e) 150°, and (f) 180°.

of values on the radial axis where the singlet exchange potential can become complex [9]. For energies greater than about 22 eV the potential is always real; for energies below this we have replaced the complex potential by zero. We note that for the cases we consider here, there is only a narrow range on the radial axis where this is necessary. Once we add polarization, the potential is always real.

It would be valuable to perform an exact exchange calculation; however, we note that even for very low-energy impact ionization the local exchange potential has been shown to compare quite well with the exact exchange [1]. The approximation as considered here still does not take account of the postcollisional interaction (PCI). Following our earlier work [2], we consider the following approximation:

$$\frac{d^3\sigma}{d\Omega_s d\Omega_f dE} = N_{ee}\frac{d^3\sigma^{\mathrm{DWBA}}}{d\Omega_s d\Omega_f dE}, \tag{5}$$

where the Gamow factor N_{ee} [1,6] is given by

$$N_{ee} := \frac{\gamma}{e^{\gamma}-1}, \quad \gamma := \frac{2\pi}{\|\mathbf{k}_s - \mathbf{k}_f\|}. \tag{6}$$

The N_{ee} factor tends to give the dominant angular behavior of the TDCS at low energies due to final state electron-electron interaction. Unfortunately the overall normalization of the theoretical TDCS is lost. Approximation (5) has the advantage, however, that we can switch the physical effects on and off at will, and this helps us to focus on different kinematical regimes where one effect is dominant. We remark that an alternative form of the Gamow factor is given by Ward and Macek [10]. This will not significantly affect the angular distribution given by using (6), but will alter the normalization. We hope to discuss the Ward-Macek factor in a later publication.

III. PCI, DISTORTION AND POLARIZATION IN DIFFERENT KINEMATICAL ARRANGEMENTS

A. Coplanar constant ϑ_{sf} geometry

Clearly it is of interest to try to investigate the role of the polarization potential. Whelan and co-workers [2,3] pointed out that the geometrical nature of N_{ee} is such that it depends only on the angle between the two outgoing electrons. By holding this fixed and rotating both about the beam direction,

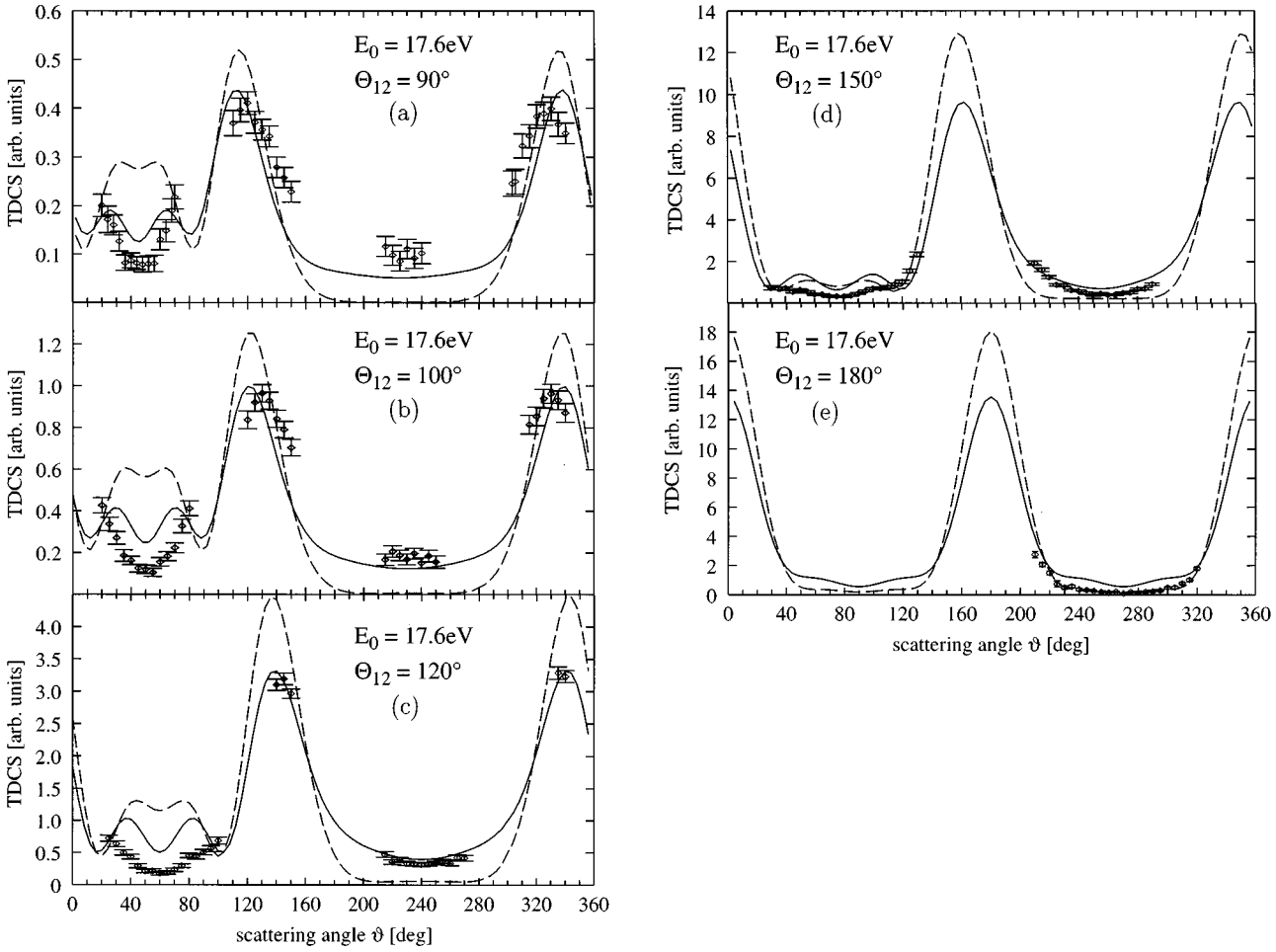

FIG. 5. TDCS in coplanar energy sharing geometry at an impact energy of $E_0 = 17.6$ eV. Experimental data are internormalized but relative, therefore all experimental data are scaled by the same overall factor to give the best fit to theory. Curves in all figures: (a) DWBA with polarization and PCI effects included (solid line); and (b) standard DWBA with PCI effects included (dashed). Both calculations are scaled by the N_{ee} factor such that the TDCS is given in arbitrary units. The angle between the two outgoing electrons is fixed at angles of (a) 90°, (b) 100°, (c) 120°, (d) 150°, and (e) 180°.

one hopes to obtain some insight into the role of three-body effects in the incident channel. In other words, if we assume that the e-e repulsion in the final state can, to a first approximation, be represented by the N_{ee} factor, i.e. a purely geometrical term, then keeping the angle constant will keep the PCI effects constant.

1. Experimental apparatus

We have performed a series of measurements in this coplanar constant geometry. The coincidence method and electron spectrometers have been described in detail previously [11]. For the measurements reported here the electron gun and the analyzer have been arranged in coplanar geometry. The electron beam is formed in the electron gun with an intensity at about 350 mA and an energy spread of 180 meV [full width at half maximum (FWHM)]. In order to obtain a well-defined shape the electron beam is monitored by a Faraday cup with inner and outer electrodes which could be moved out of the way for measurements at forward angles. The background of low-energy secondary electrons is reduced by collecting the unscattered electron beam with a large-scale Faraday cup.

The target beam emerges from a nozzle of 1 mm in diameter perpendicular to the scattering plane, and is 2 mm above the nozzle intersected by the electron beam forming the scattering region. The two electrons emerging out of the scattering region are detected in coincidence using two identical double-cylindrical 127° analyzers. The smallest angle between the two analyzers is 40°, and both detectors can reach a backward angle of 150° and 148°, respectively. The angular acceptance profile of the system has a width of about $\pm 3.5°$. Each analyzer has a bandwidth of about 260 meV leading to a coincidence resolution of about 360 meV. All systems are heated up to 130–200 °C during operation, giving a long-term stability of the experiment. No readjustments of the beam deflection spectrometer optics were necessary during measurement of an angular distribution within one or two days.

Atomic hydrogen is produced in a microwave dissociation located outside the vacuum chamber. The microwave cavity encloses a glass tube in which the discharge operates with a power of 150 W at a pressure of 1 mbar. The glass tube is cooled by using compressed air of about -10 °C.

The final test of the alignment of the system was made prior to all coincidence measurements by interchanging the

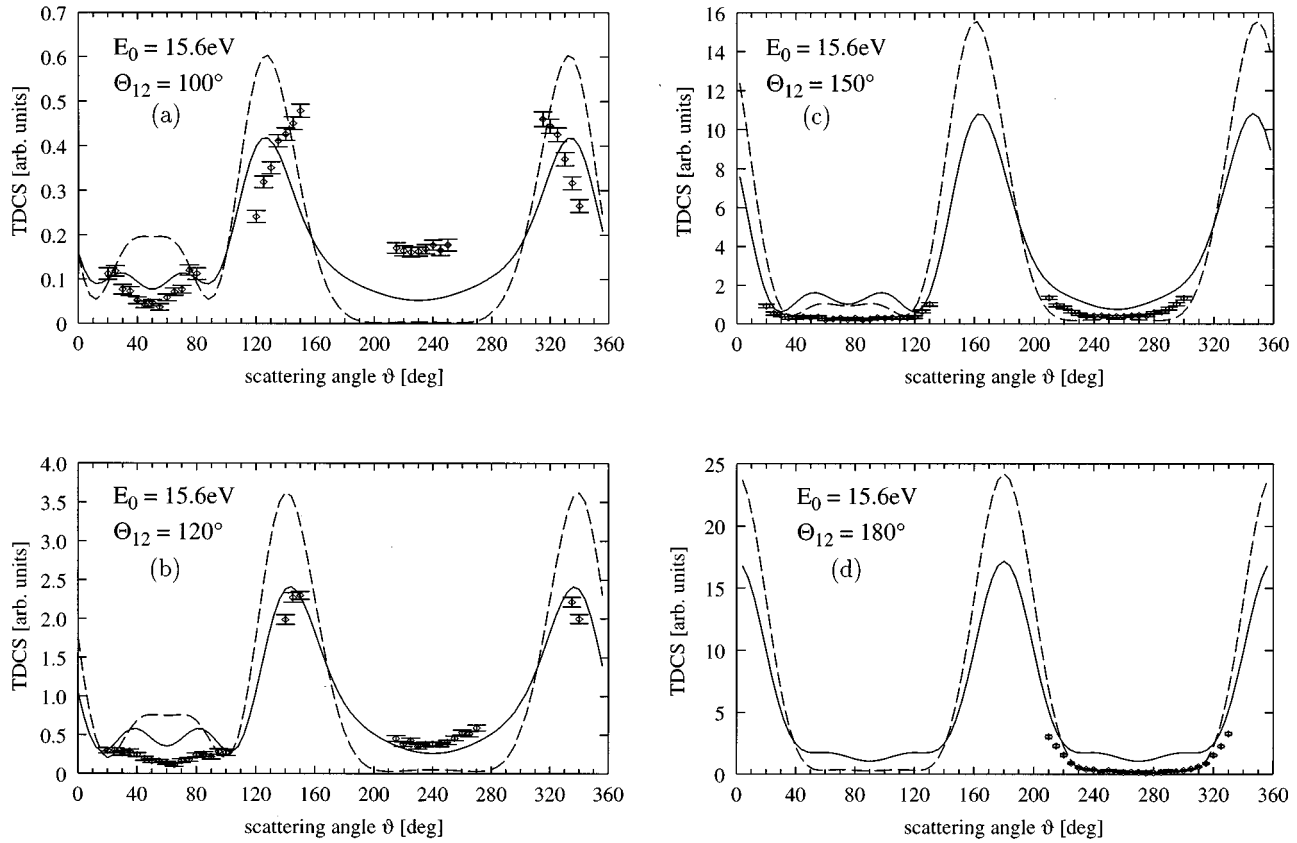

FIG. 6. TDCS in coplanar energy sharing geometry at an impact energy of $E_0 = 15.6$ eV. Experimental data are internormalized but relative, therefore all experimental data are scaled by the same overall factor to give the best fit to theory. Curves in all figures: (a) DWBA with polarization and PCI effects included (solid line); and (b) standard DWBA with PCI effects included (dashed). Both calculations are scaled by the N_{ee} factor such that the TDCS is given in arbitrary units. The angle between the two outgoing electrons is fixed at angles of (a) 100°, (b) 120°, (c) 150°, and (d) 180°.

position of the two analyzers, which should always lead to the same value of true coincidences in the case of equal energies for the two electrons. The statistical errors of the experimental data are on the order of 30% in the minima of the cross section, and less than 7% for the most intense data points.

All measurements are on a relative scale, but for each impact energy the different angular dependences are normalized to one another. In the case of 30-eV impact energy this internormalization introduces a relative error of less than 15%; in all other cases it is less than 10%.

2. Comparison with theory

The experimental data are internormalized at a given energy, but not on an absolute scale. We have therefore multiplied the triple-differential cross section for a given constant ϑ_{sf} by the constant N_{ee} factor to take account of the diminishing yield for smaller ϑ_{sf} angles. We then chose an overall factor to give the best agreement with experiment at a given energy.

In Fig. 1 we show the TDCS as a function of ϑ_s in coplanar constant geometry at an impact energy of 25 eV for a fixed ϑ_{sf} of 90°. $\vartheta_s = 0$ and $\vartheta_f = 90$ correspond to one electron detector lying in the beam direction. Shown are the DWBA, DWBA plus polarization, and a series of model calculations where we switch on and off the interactions in the various channels. If we replace the incident distorted waves by a plane wave but retain the Coulomb waves in the final channels, we have a Coulomb-projected Born exchange approximation (CPBX) [12,13], and if we retain distortion in the incident channel but use orthogonalized plane waves for the outgoing electrons then we have a plane-wave–distorted-wave calculation (PW-DW) [14]. We remark that at the symmetric point the triplet terms no longer contribute, so we have pure singlet scattering. The latter two calculations are nonrealistic, but they allow us to assess the relative importance of nuclear versus final channel effects and their interference.

Since we are dealing with an energy sharing problem, the cross section must be symmetric about $\vartheta_s = \frac{1}{2}\vartheta_{sf}$. In the case of the PW-DW approximation we observe two peaks, one centered at $\vartheta_s = \frac{1}{2}\vartheta_{sf} = 45°$, which we will refer to as the primary, and one at 105° which we will call the secondary [3]. In the CPBX approximation, the primary peak splits in two around the symmetric point. Both the primary and secondary peaks are enhanced, but the ratio of primary to secondary is greatly increased.

Replacing the incident plane wave in the CPBX by a distorted wave generated in the static exchange potential of the atom (i.e., the standard DWBA) only produces a slight ef-

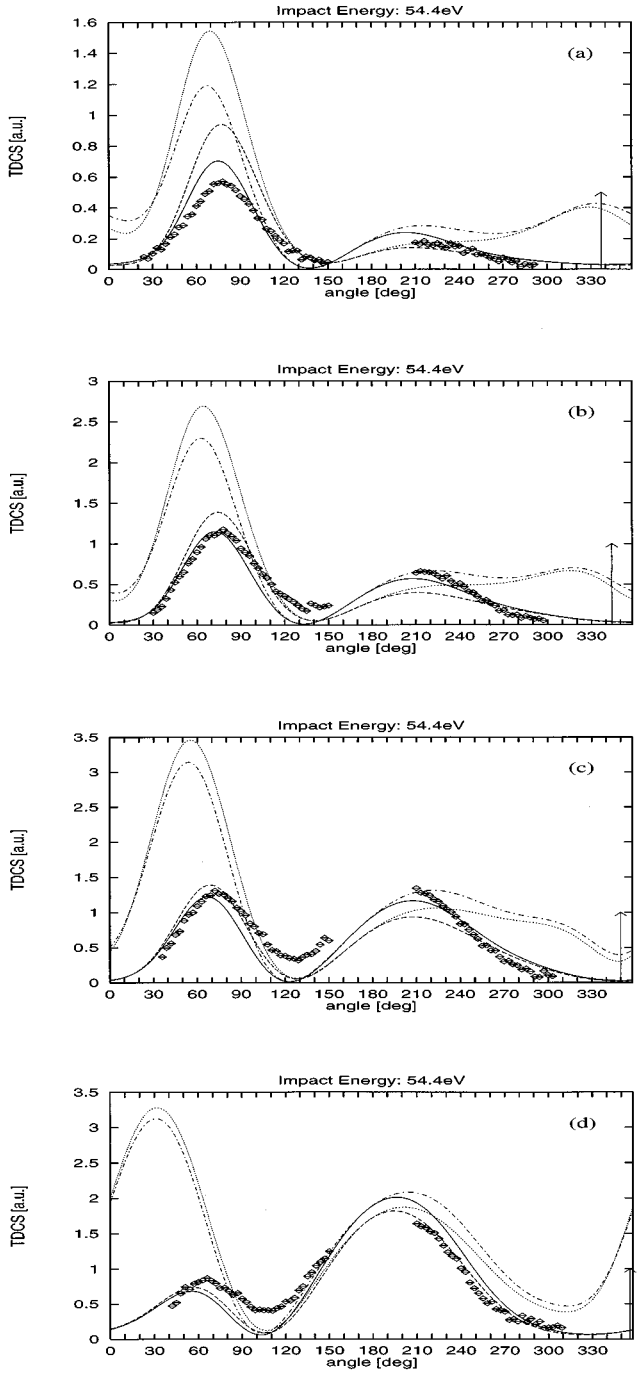

FIG. 7. TDCS in coplanar asymmetric geometry at 54.4 eV; the energy of the slow outgoing electron is 5 eV. Shown is the standard DWBA with neither polarization nor PCI effects included (dotted line); DWBA with polarization but no PCI (dashed-dotted); DWBA with PCI but no polarization (dashed); and DWBA with both polarization and PCI (solid line). The angle of the fast electron fixed at (a) 23°, (b) 16°, (c) 10°, and (d) 4°. Experimental data are internormalized at this energy. The TDCS of the DWBA and DWBA plus polarization calculations are given in a.u., and all other curves are scaled. The arrow denotes the scattering angle of the fast electron.

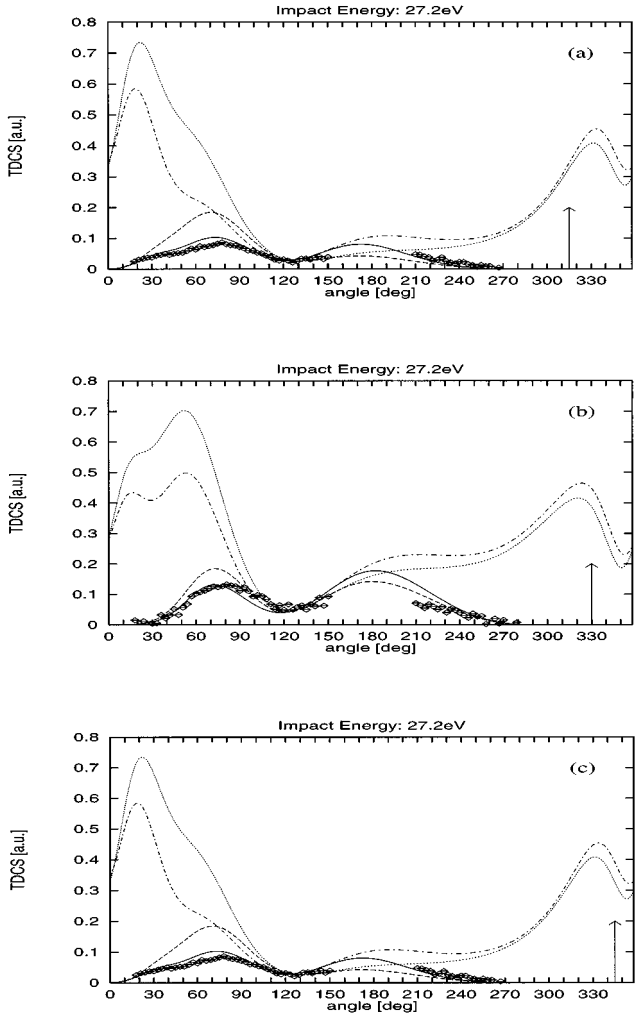

FIG. 8. TDCS in coplanar asymmetric geometry at 27.2 eV; the energy of the slow outgoing electron is 6.8 eV. Shown is the standard DWBA with neither polarization nor PCI effects included (dotted line); DWBA with polarization but no PCI (dashed-dotted); DWBA with PCI but no polarization (dashed); and DWBA with both polarization and PCI (solid line). The angle of the fast electron fixed at (a) 45°, (b) 30°, and (c) 15°. Experimental data are internormalized at this energy. The TDCS of the DWBA and DWBA plus polarization calculations are given in a.u., and all other curves are scaled. The arrow denotes the scattering angle of the fast electron.

fect. However the inclusion of the strong adiabatic polarization potential has a significant influence on the primary peak. In Figs. 2–6 we show a comparison of theory and experiment for a series of energies and fixed angles; Only the DWBA and DWBA plus polarization are shown. We see at once that it is the region around the primary peak where the influence of the polarization potential is most strongly felt; it is also this region where the greatest discrepancy between theory and experiment is observed. For the secondary peak we have good accord between both the distorted-wave approximations, and also have satisfactory agreement with experiment. We note that the minimum between the primary and secondary peaks is not accessible to measurement; however, there is some indication of it in our experimental results. At lower energies, especially at 17.6 and 15.6 eV, DWBA and DWBA plus polarization disagree for both primary and secondary peaks, and only poorly reproduce the experimental results. We may speculate that at these low energies it is no longer reasonable to maintain the separability of the incident, final-channel effects; i.e., PCI can no longer

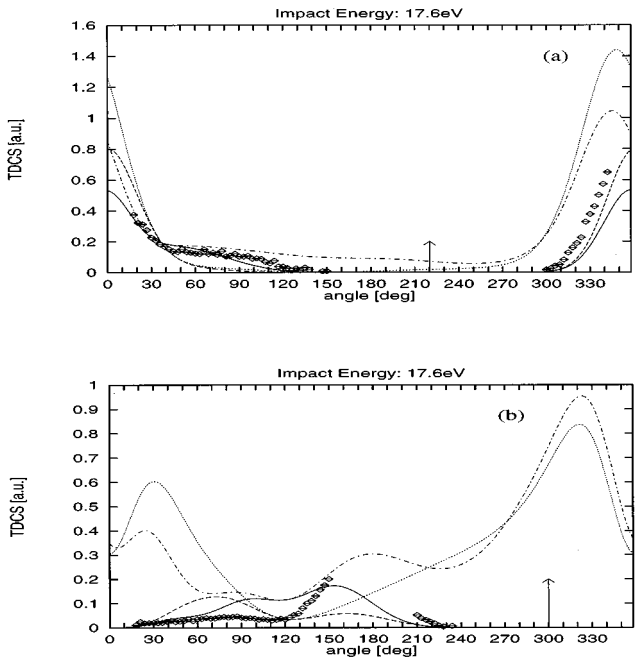

FIG. 9. TDCS in coplanar asymmetric geometry at 17.6 eV; the energy of the slow outgoing electron is 2.0 eV. Shown is the standard DWBA with neither polarization nor PCI effects included (dotted line); DWBA with polarization but no PCI (dashed-dotted); DWBA with PCI but no polarization (dashed); and DWBA with both polarization and PCI (solid line). The angle of the fast electron fixed at (a) 140° and (b) 60°. Experimental data are internormalized at this energy. The TDCS of the DWBA and DWBA plus polarization calculations are given in a.u., and all other curves are scaled. The arrow denotes the scattering angle of the fast electron.

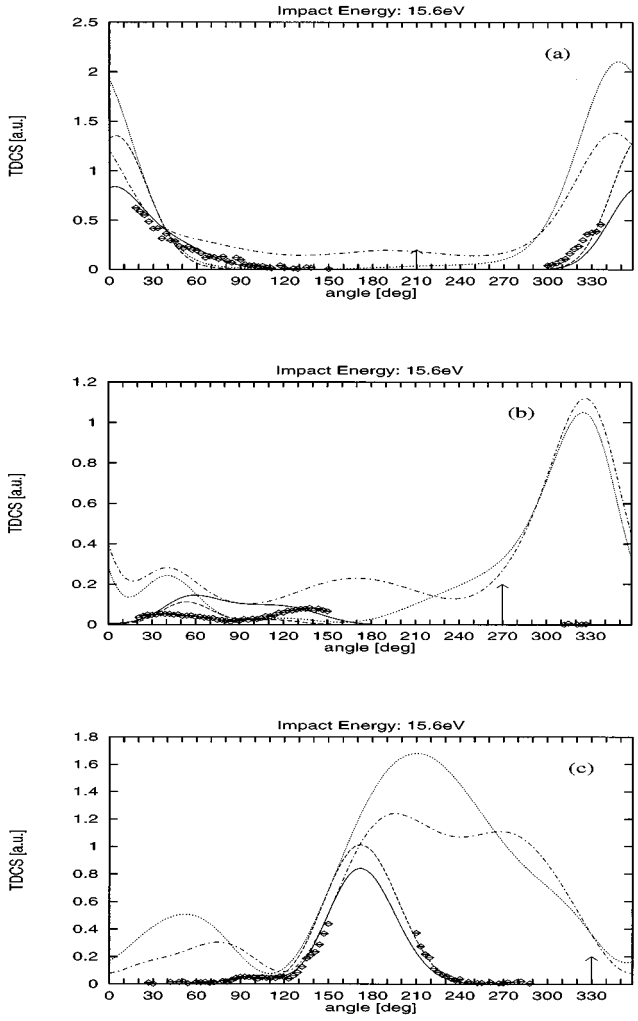

FIG. 10. TDCS in coplanar asymmetric geometry at 15.6 eV; the energy of the slow outgoing electron is 1.0 eV. Shown is the standard DWBA with neither polarization nor PCI effects included (dotted line); DWBA with polarization but no PCI (dashed-dotted); DWBA with PCI but no polarization (dashed); and DWBA with both polarization and PCI (solid line). The angle of the fast electron fixed at (a) 150°, (b) 90°, and (c) 30°. Experimental data are internormalized at this energy. The TDCS of the DWBA and DWBA plus polarization calculations are given in a.u., and all other curves are scaled. The arrow denotes the scattering angle of the fast electron.

be regarded as a geometrical effect.

B. Coplanar asymmetric geometry

We have calculated cross sections for a range of energies in this geometry, and compare our results with the earlier experimental results [11]. In coplanar asymmetric geometry one electron, usually the faster one, is detected at a given fixed angle with respect to the incident beam, and the TDCS is given as a function of the second electron angle. For a given impact energy the experimental TDCS's are not absolute, but internormalized for different scattering angles of the fast electron. The experimental data are, therefore, rescaled to the theory by multiplying them by an overall factor for a given energy to give the best agreement with experiment. In Figs. 7–10 we compare theory with experiment at a range of impact energies. Since, as mentioned above, the effect of the N_{ee} factor is to destroy normalization, we arbitrarily scaled our results as follows: We redefined N_{ee} as $N_{ee}=N_{ee}(\vartheta)/N_{ee}(180°)$, where $N_{ee}(180°)$ is $N_{ee}(\vartheta)$ evaluated when the angle between the two outgoing electrons is 180°.

We find that again both polarization and PCI effects are needed to obtain good agreement with experiment, at least for higher energies. However, we see that the N_{ee} factor has a more profound effect on the TDCS than the polarization potential in the incident channel. We could interpret this as PCI dominating over polarization in this geometry. Indeed, when one sees a strong influence of the polarization (e.g., $E_0=17.6$ eV, $\vartheta_f=60°$ and $E_0=15.6$ eV, $\vartheta_f=90°$) one obtains only poor agreement with measurement.

At 54.4 eV there are coupled-channel calculations due to Curran and Walters [15] and, more recently, Bray, Konovalov, and McCarthy [16]. In particular, the latter calculation gives good accord with the data at this energy. Such calculations are unavailable for lower energies.

C. Coplanar symmetric geometry

This arrangement was considered in our earlier paper [2], where it was shown that good agreement with measurements could be achieved for impact energies of 20 eV and above if and only if both the polarization and PCI were included. At energies below 20 eV, experiment and theory diverged with

theory, becoming progressively more Wannier-like, i.e., a single peak at angle of 180° between the two outgoing electrons, while the experiment continued to display a more complex structure right down to an impact energy of 14.6 eV.

IV. CONCLUSION

In our earlier paper [2], we showed that coplanar symmetric geometry at low energies on H could not be understood if one did not take into account three-body effects in both the incident and final channels. The object of this present work was to look for geometrical arrangements where either the incident or final channels were dominant. It is our belief that they have been identified. Within the confines of a simple model, we have shown the coplanar constant ϑ_{sf} geometry to be ideal for studying incident channel effects, while final-channel PCI's are strong in asymmetric geometry.

[1] Colm T. Whelan, H. R. J. Walters, and R. J. Allan, J. Phys. (France) IV **3**, C6–39 (1993).
[2] Colm T. Whelan, R. J. Allan, J. Rasch, H. R. J. Walters, X. Zhang, J. Röder, K. Jung, and H. Ehrhardt, Phys. Rev. A **50**, 4394 (1994).
[3] Colm T. Whelan, H. Ast, H. R. J. Walters, S. Keller, and R. M. Dreizler (unpublished).
[4] M. L. Goldberger and K. M. Watson, *Collision Theory* (Wiley, New York, 1964).
[5] Colm T. Whelan, R. J. Allan, H. R. J. Walters, and X. Zhang, in *(e,2e) and Related Processes*, edited by Colm T. Whelan, H. R. J. Walters, A. Lahman-Bennani, and H. Ehrhardt (Kluwer Academic, Dordrecht, 1993).
[6] H. R. J. Walters, X. Zhang, and Colm T. Whelan, in *(e,2e) and Related Processes* (Ref. [5]).
[7] M. J. Seaton, Proc. R. Soc. London **245**, 469 (1953).
[8] J. B. Furness and I. E. McCarthy, J. Phys. B **6**, 2280 (1973).
[9] M. E. Riley and D. G. Truhlar, J. Chem. Phys. **65**, 792 (1976).
[10] S. J. Ward and J. H. Macek, Phys. Rev. A **49**, 1049 (1994).
[11] M. Brauner, J. S. Briggs, H. Klar, J. T. Broad, T. Rösel, K. Jung, and H. Ehrhardt, J. Phys. B **24**, 657 (1992).
[12] S. Geltman and M. B. Hidalgo, J. Phys. B **7**, 831 (1974).
[13] Colm T. Whelan, H. R. J. Walters, J. Hanssen, and R. M. Dreizler, Aust. J. Phys. **44**, 39 (1991).
[14] X. Zhang, Colm T. Whelan, H. R. J. Walters, R. J. Allan, P. Bickert, W. Hink, and S. Schönberger, J. Phys. B **25**, 4325 (1992).
[15] E. P. Curran and H. R. J. Walters, J. Phys. B **20**, 337 (1987).
[16] Igor Bray, Dmitry A. Konovalov, and Ian E. McCarthy, Phys. Rev. A **50**, R2818 (1994).